Odour mapping and air quality analysis of a wastewater treatment plant at a seaside tourist area

Andreas Luckert[a], Daniel Aguado[b,**], Rafael García-Bartual[b], Carlos Lafita[c], Tatiana Montoya[c], and Norbert Frank[a]

[a] *Institute of Environmental Physics, Heidelberg University, Heidelberg, Germany*
[b] *Institut Universitari d'Investigació d'Enginyeria de l'Aigua i Medi Ambient – IIAMA, Universitat Politècnica de València, Camí de Vera s/n, 46022 Valencia, Spain.*
[c] *Global Omnium Medioambiente S.L., Avenida Marqués del Turia 19, 46005, Valencia, Spain*

* This document is the result of the collaborative research project between the Universitat Politècnica de València (Spain) the Heidelberg University (Germany) and the wastewater utility Global Omnium Medioambiente S.L.
** Corresponding author: daaggar@hma.upv.es

Abstract

Although wastewater treatment plants (WWTPs) play a fundamental role in protecting the aquatic environment as they prevent organic matter, nutrients and other pollutants from reaching the natural ecosystems, near to residential areas they can generate unpleasant smells and noise. The plant studied in the present work is in a seaside tourist area in the Valencian Community, Spain. The main aim was to detect any possible perceptible H_2S concentrations from the WWTP by experimental measurement campaigns (including sensor readings and olfactometry measurements by two experts) plus mathematical modelling. After a thorough data analysis of the essential variables involved, such as wind speed, wind direction and H_2S concentrations (the main odorant) and comparing their temporal patterns, it was found that the probability of affecting the residential area was highest from June to August before noon and in the late evening. The hourly H_2S concentration, influent flow rate and temperature showed a positive correlation, the strongest (R^2=0.89) being the relationship between the H_2S concentration and influent flow rate. These two variables followed a similar daily pattern and indicated that H_2S was emitted when influent wastewater was being pumped into the biological reactor. The H_2S median concentration at the source of the emission was below 1393.865 $\mu g/m^3$ (1 ppm), although concentrations 10 times higher were occasionally recorded. The observed H_2S peak-to-mean ratio (1 min to 1 hour of integration times) ranged from 1.15 to 16.03. This ratio and its attenuation with distance from the source depended on the atmospheric stability. Both H_2S concentrations and variability were considerably reduced after submerging the inlet. The AERMOD modelling framework and applying the peak-to-mean ratio were used to map the peak H_2S concentration and determine the best conditions to eliminate the unpleasant odour.

***Keywords*:** air quality, dispersion modelling, hydrogen sulphide, odour map, wastewater treatment, WWTP.

1. Introduction

Unpleasant smells (odorants) from wastewater treatment plants (WWTPs) can be a public nuisance (Zounemat-Kermani *et al.*, 2019), with the logical complaints from nearby residents (Dinçer *et al.*, 2020). Odour nuisance negatively affects the quality of life and can be a source of various negative health issues, despite not being linked to any specific disease (World Health Organization, WHO 2000; Piccardo *et al.*, 2022). Odour is currently classified as an atmospheric pollutant to be minimized to reduce its impact (Toledo *et al.*, 2019). Unpleasant WWTP smells have given great concern for years, especially in communities with high population densities (Fan *et al.*, 2020).

The proteins and fats in the organic compounds in wastewater decompose in the absence of oxygen, producing H_2S, NH_3, methyl mercaptan, amines, and other odorous gases as well as volatile organic compounds (VOCs) such as toluene, butyl acetate and styrene (Liu *et al.*, 2021). According to Halageri (2012) and Carrera-Chapela *et al.* (2014), odorants originate from the microbial decomposition of organic compounds of high molecular weight, especially proteins. Anaerobic fermentation involving hydrolysis and acidogenesis is an important precursor to other anaerobic processes that transform large, complex organic molecules into smaller, simpler molecules that can be directly used by other microorganisms as a substrate. The organic products in anaerobic hydrolysis do not generally emit odours from sewers, with the exception of the hydrolysis of organic sulphur-containing compounds by bacteria, resulting in the production of hydrogen sulphide (H_2S), organic sulphides and disulphides. Most of the unpleasant smells are related to sulphide-derived compounds, such as H_2S, the principal odour-causing component.

According to Shareefdeen and Singh (2005), common odour problems are generally caused by mixtures of highly volatile organic (VOCs) and inorganic compounds (VICs, such as H_2S) with very low threshold perception limits. The H_2S odour detection threshold has been determined in many laboratory studies, reporting variable concentrations (from 0.47 µg/m^3 to higher than 100 µg/m^3), although no threshold value has been reported. Human responses to odours vary widely. People regularly exposed to high levels of ambient H_2S (e.g., in the vicinity of areas with geothermal activity) have greater tolerance to odours and a reduced sensitivity to its detection (Iremonger, 2012). According to the WHO air quality guidelines (2000), concentrations exceeding 7 µg/m^3 are likely to produce substantial complaints from nearby residents. Several studies have identified VOCs and H_2S as being the major odours from sewer-pipes and aerobic WWTPs (Smet *et al.*, 1998), with various short- and long-term adverse health effects (Shareefdeen and Singh, 2005)

As indicated by Halageri (2012), apart from the predominating VOCs, other odorants with a hazardous effect on people's health can be identified. Shareefdeen and Singh (2005) found that inorganic gases, known as volatile inorganic compounds (VICs), include H_2S and ammonia (NH_3), which are considered to be the main causes of these smells and were the odorants studied in this project.

According to the Agency for Toxic Substances and Disease Registry (ATSDR, 2016), H_2S is a flammable, colourless gas that smells like rotten eggs and has a very low perception threshold in the same order of magnitude as several VOCs produced by fermentation (Hvitved-Jacobsen *et al.*, 2002). It has a component with a relatively high Henry's law constant, i.e. H_2S has a relatively high tendency to evaporate in the wastewater phase as a malodourous airborne substance. Many studies (Hvitved-Jacobsen *et al.* 2002; Pikaar *et al.* 2014; Li *et al.* 2019) have found that H_2S is directly related to the corrosion in sewage networks and can cause serious human health problems.

Badach *et al.* (2018) concluded that the effective management of unpleasant odours in urban environments requires reliable odour emission evaluation and the determination of its range. These authors also highlight the importance of objective odour impact evaluation due to the complexity of directly determining odour nuisance. Zhang *et al.* (2020) point out the importance of aesthetic indicators like smells because they are of major concern for public acceptability. These authors state that no odour nuisance should be associated with water facilities, especially in urban applications, but that odour quantification studies in wastewater infrastructures are still limited. Lewkowska *et al.* (2016) indicate the usefulness of field olfactometry to quantify WWTP and landfill odours to identify the source and determine their intensity. Dispersion modelling is considered to be the most effective approach to evaluating the impact of odours (Mott and Guo, 2022), using field data to calibrate the model.

This paper describes the results obtained in applying a method of assessing odours based on odour mapping by the Gaussian AERMOD modelling framework, with on-site concentration measurements. Two different types of point sources were considered including various local surface meteorological data and vertical atmospheric profiles along with complex terrain data from regional LIDAR-based digital elevation models (DEMs). The AERMOD atmospheric dispersion model combined with an empirical peak-to-mean ratio enables the diagnosis and prediction of odorant concentrations in complex terrain and has been effectively used for this purpose (Oliveira and Corrêa, 2022). The results can determine whether mitigation measures are necessary to protect an adjacent residential area from perceivable or even hazardous odorant concentrations. This method can be directly applied to other WWTPs with different sizes, process configurations and wastewater compositions.

2. Materials and methods

2.1. Description of the WWTP

Figure 1 depicts an aerial view of the WWTP next to the beach in a tourist residential area in the south of

Valencia, Spain, belonging to the Valencia public wastewater management association. Its most important components can be seen in Figure 1b along with the immediate vicinity. The wastewater treatment process is as follows: wastewater is pumped directly from the underground sewer pipes into the bioreactor, which cultivates microorganisms to break down the organic material in aerobic conditions. The next step is the decanter connected to the bioreactor in which the activated sludge flocks settle. To maintain the proper concentration of microorganisms in the system, the sludge settled on the bottom of the decanter is regularly extracted and partially recirculated into the bioreactor to sustain the appropriate biomass associated with the level of microorganisms. The water leaving the decanter is disinfected and is then ready for renaturation or further use. The extracted sludge is sent to the drying basins, except in the summer between 15 June and 15 September, a period in which the number of temporary holiday residents significantly increases. Further sludge processing is outsourced to a large centralized WWTP to avoid its presence and associated emissions.

(a) (b)

Figure 1. (a) Aerial view of the WWTP and surrounding residential area. **(b)** Close-up of the WWTP showing its main components. The entry pipe (main emission source) is marked by a red cross and the olfactometric measurement points are in sequentially numbered blue circles.

The area of the 7 sludge drying beds totals 11 m x 5 m, the diameter of the bioreactor measures 22 m and the decanter comprises a diameter of 12 m. Information on the GPS and the elevation data necessary for modelling was obtained from Google Maps Coordinates. The height above sea level of the emission source is 4 m. The projected wastewater flow rate is 628 m^3/d and the total power of the installation is 49 kW. The specific data given here were from the year 2018 when volume flow rate averaged 226 m^3/d and served a population equivalent (PE) of 1116. 1 PE is defined as 60g BOD_5/d. PE is the reference used to evaluate the organic polluting load of industrial or other waste in a WWTP or stream. Suspended solids removal was 92 %, 5-day biochemical oxygen demand removal was 95 % and chemical oxygen demand removal was 92 %.

2.2. Instrumentation

Two gas detectors (*Dräger Polytron 7000)* were deployed in both measurement campaigns (2018 and 2019) to measure odorant concentrations at various points in the WWTP, including the emission source, the edge of the bioreactor opposite the dwellings and the sludge drying basins. Sensors were installed every 10 m along the wall facing the residential area. The campaigns were carried out between July and October 2018 and from April till August 2019, since the odour problems are usually higher in summer with increased resident numbers. The higher population in summer means both higher wastewater flows into the WWTP and a higher susceptibility risk and the complete occupation of the buildings around the WWTP.

The Polytron 7000 can record a maximum of one measurement per minute. The measured values were saved in an external register connected via cable. The following specifications are applicable to typical values within the measuring range of new sensors in ambient conditions of 20 ºC (68 ºF), 50 % relative humidity and 1013 mbar. The accuracy of the H_2S readings is either ±3 % or ±139 μg/m^3, whichever is higher. The reliable measuring range is from 0 to 139388 μg/m^3.

Apart from hydrogen sulphide, the Polytron 7000 also measured NH_3, but this was not considered in the model as its concentration remained well below the human perception threshold at all the measuring points (maximum measured concentration per minute at the inlet was 2160 μg/m^3, although most of the time the inlet concentration per minute remained below 1045 μg/m^3, while the perception threshold for this compound is 3482 μg/m^3). The measurement accuracy for NH_3 was either ≤ ±5% or ≤ ±1045 μg/m^3, whichever is greater, while the reliable measuring range is from 0 to 208957 μg/m^3.

Field measurements were carried out on a Field olfactometer Nasal Ranger® by two calibration experts belonging to the Global Omnium Medioambiente S.L. company on 10 days during both campaigns. The gas detectors were placed in the same locations and at various points on the footpath outside the WWTP. The odour concentrations were measured in European Odour Units (OU_E)/m^3 categorized from 1-5 in odour intensity. Odour values above 15 OU_E/m^3 belong to the intensity Group 5, which indicates maximum unpleasantness.

According to Walgraeve *et al.* (2015), the Nasal Ranger® generates a series of discrete dilutions by mixing odorous air with odour-free air, using the breathing rate of the panellist to mix the odorous air with the odour-free air generated by carbon filtration of odorous air. The different dilution-to-threshold (D/T) positions were 60, 30, 15, 7, 4 and 2. D/T was defined as the ratio of carbon-filtered to odorous airflow.

2.3. Modelling framework

According to EPA and AERMIC (2019), the AERMOD modelling system is a steady-state Gaussian plume model that incorporates air dispersion based on the planetary boundary layer turbulence structure and scaling concepts, including treatment of both surface and elevated sources in both simple and complex terrain. The workflow includes pre-processor models to prepare the terrain (AERMAP) and meteorological data inputs (AERMET and AERSURFACE), as well as possible downwash effects (BPIPPRM) caused by buildings close to the emission source. According to Dinçer *et al.* (2020), AERMOD is one of the Gaussian models employed for applications like the present work because of its reliable near-field performance. Our aim was not to model air pollutant propagation around the buildings (a model requiring the explicit treatment of buildings would be necessary), but to assess any WWTP odours in the vicinity reaching the buildings (at the perceptible concentration) emitted by the WWTP, as the area is fairly flat with low-rise buildings. The study focused on a small domain in which the WWTP was the only source of emissions. Dispersion modelling by AERMOD has been used in other WWTP studies to predict odour dispersion (e.g., Baawain *et al.,* 2017; Fileni *et al.*, 2018; Dinçer *et al.*, 2020).

We used a rectangular 6400-point receptor grid with 2.5 m x 2.5 m cells and a total edge length of 200 m. Since the AERMOD maximum time-resolution is 1 hour, all the gas and meteorological data were resampled with a higher temporal resolution than the target resolution. Taking the hourly maximum was the chosen aggregation function for the gas data, as the worst-case scenario was the most relevant in this work. If the mean or median had been used, the hourly H_2S concentrations would have remained below the perception threshold due to intermittent wastewater pumping into the bioreactor, which takes place approximately every 1-2 minutes and lasts around 15 seconds. The hourly mean of the surface meteorological data was considered for all the variables of interest, such as wind direction, wind speed and temperature.

The AERMOD results provide an estimation of average concentrations, while odours are detected at peak concentration values in periods of less than 1 minute, so that the AERMOD concentration field cannot provide information on their occurrence. To solve this issue and obtain more realistic predictions, the empirical method based on the peak-to-mean ratio was applied to the concentration field obtained by the mathematical model (Oliveira and Corrêa, 2022). The most widely used equation to estimate concentrations at shorter intervals from values produced by dispersion models in longer average periods (Nicell, 2009) was thus used: $C_p=C_m(t_m/t_p)^n$, C_m and C_p being the mean and peak concentrations for the longer and shorter times, respectively and t_m and t_p the longer (i.e. mean) and the shorter (peak) average times, respectively, and n a dimensionless exponent dependent on the degree of atmospheric turbulence (stability) and typically ranging from 0.17 to 0.68. The effect of atmospheric stability on this empirical exponent and on the attenuation of the peak-to-mean ratio with the distance from the odour-emitting source has been studied and can be found in Schauberger *et al.*, 2000; Piringer *et al.*,2015; Piringer *et al.*, 2019; Brancher *et al.*, 2020.

In the present study, the peak-to-mean ratio was empirically obtained from the recorded 1-minute H_2S concentration values and their corresponding 1-hour averages. The power-law function was then used to estimate peak concentrations at 4 seconds (the duration of a single breath at the normal respiration rate) from the 1-minute H_2S concentrations produced by AERMOD (as the hourly maximum from the recorded H_2S concentrations (1 value per minute) was the aggregation function of choice for the AERMOD gas data).

The options used in AERMOD included stack-tip downwash, elevated terrain effects, the processing routine for no wind, the missing data processing routine and no exponential decay. No gas and particle deposition and no dry or wet depletion were included. A flagpole height of 1.7 m was used for all the receptor points of the modelling grid to compute the results for the height of an average person. Owing to the unstable surface atmospheric conditions in summer, this height is also representative of houses of up to two storeys. Rural dispersion was chosen as the target residential area at around 300 m from the coast with relatively low building density and height. As the emission source type was changed from an open-air outlet pipe to a submerged inlet from 2018 to 2019 (Figure 2), different model parameters had to be considered. Until 2018 the pipe pointed down towards the water surface, where a screening grate filtered out coarse objects (Figure 2a). The pumping cycle had a frequency of around every 1 or 2 minutes in the high summer season, causing turbulence in the falling water with considerable splashing owing to the metal grate underneath. The most accurate POINTHOR point emission source type was therefore selected instead of the standard POINT for the AERMOD modelling procedure. If the latter had been chosen, the model would have assumed a point source with the opening pointing upwards.

A new WW inlet pipe was installed during the second measuring campaign in 2019, comprising a submerged inlet pipe into the bioreactor with previous filtering through a rotary sieve (Figure 2b). This sieve is overground and partially capped to prevent a direct gas stream from the outlet, although it is also open to the atmosphere, so that the POINTCAP source type was chosen.

(a) **(b)**

Figure 2. Views of the bioreactor inlet pipe: **(a)** open-air inlet discharging directly onto the bioreactor screen during the first measuring campaign: **(b)** submerged inlet to avoid splashing and the release of dissolved gases during the second measuring campaign.

Regarding the point source input data, the 2018 installation consisted of an average mass emission rate of between approximately 0.14 and $0.22 \cdot 10^{-4}$ g/s, depending on the modelling period, a stack height of 0.3 m, an average temperature of between around 296 and 300 K, a stack velocity of between 0.09 and 0.24 m/s and an opening vent diameter of 0.16 m, while in 2019 the emission source had an average mass emission rate of $0.94815 \cdot 10^{-8}$ g/s, stack height of 1.25 m, an average temperature of 290.63 K, a stack velocity of 0.00 m/s and an opening vent diameter of 0.20 m. The currently inserted value of the stack exit velocity was around $7 \cdot 10^{-5}$ m/s, which was rendered as 0 by AERMOD.

2.4. Meteorological data

The upper air sounding data were obtained from the Integrated Global Radiosonde Archive (NOAA, a) while the hourly weather stations lie either on the coast or within 3 km of it. The cloud surface data are issued by the global Integrated Surface Dataset (NOAA, b). The latter data were complemented by other local surface weather stations in the Valencian AVAMET network (see Figure 3). The AVAMET's Dénia Platja de Pego weather station is the closest surface weather station to the WWTP site, the second closest is Oliva Poble, along with the Platja de Piles Windguru station between Gandia and Oliva, and the Windguru station Playa de l'Ahuir north of Gandia. All the base height and cloud fraction data were retrieved from the Sentinel-5P TROPOMI Cloud 1-Orbit L2 data sets available from the NASA Earthdata website (NASA, 2019, 2020).

Figure 3. Map of the local surface meteorological stations used and the WWTP studied.

As can be seen in Figures 1a and 3, the studied area is in the vicinity of the coast with a land-sea breeze (LSB) causing a diurnal modulation of wind speed and direction. Basically, the LSB circulation is due to a pressure gradient force from the sea pushing a shallow layer of sea air inland, followed by a convective sea breeze cell initiated close to the coast expanding both onshore and offshore (Rafiq *et al.*, 2020). The interaction between the marine and continental air masses leads to thermal and mechanical turbulence and high variances in vertical wind fluctuations (upwelling and downwelling processes) that can become strong at a height of 1.5 km, which can foster precipitation and/or the accumulation or transfer of pollutants (Augustin *et al.*, 2020; Ma *et al.*, 2021; Rafiq *et al.*, 2020) due to affecting the boundary layer height and the conditions for vertical diffusion.

The updrafts in continental and marine air masses in the vicinity of the sea breeze front have been well described in the literature. Simulations by Talbot *et al.* (2007) indicated that they arise below 700 m with a vertical wind speed that can locally reach 1.3 m/s. The analysis of wind speed showed that the vertical compression generated by the rising sea breeze is caused about 1.3 km inland and increases the horizontal wind velocity behind the sea breeze front.

The effect on atmospheric circulation of the marine breeze in a complex coastal area happens on a mesoscale, so that the Regional Atmospheric Modelling System (RAMS) models are appropriate. In this regard, Cocci Grifoni *et al.* (2002) compared the modelling of a combined RAMS model with AERMOD and AERMOD stand-alone o assess pollutant-dispersion in Esino Valley (Italy) and found that both models can predict similar short-term average concentrations when using similar input data, although the combination of both models can be used for the special refinement of the results.

However, the present study was on the microscale, and atmospheric parameters were measured at meteorological stations close to the study area. The distance from the seashore to the WWTP is about 340 meters and clearly within the range (up to 1.3 km) reported in the literature in which upstream wind occurs. Also, the maximum distance and height with possible odour annoyance were about 40 m from the emission source and first floor, respectively. In these circumstances a steady-state Gaussian model is suitable such as AERMOD, which handles both flat and complex terrain modelling and considers turbulence and dispersion with terrain interactions. This model considers the wind speed, wind direction and turbulence parameters generated by a meteorological pre-processor (Cocci Grifoni *et al.*, 2002). Variations in atmospheric conditions were thus considered in the AERMOD modelling process.

2.5. Terrain data

The land usage and surface classification data is based on the Copernicus European Land Cover project with the CORINE Land Cover (CLC) Data Base (2018). The data are also accessible via the website of the *Centro de Descargas del Centro Nacional de Información Geográfica* (CNIG) (2018). Before passing the classified terrain data to AERSURFACE, they need to be converted to the category nomenclature of the National Land Cover data 1992 defined by the United States Geological Survey (USGS). The Digital Elevation Model (DEM) data passed to AERMAP were also downloaded from the Spanish government's CNIG website and were derived from local LIDAR satellite images. Figure 4 shows a map of the terrain with the elevation coded in colour contour lines. The 2 m high wall surrounding the WWTP was considered for possible building downwash effects.

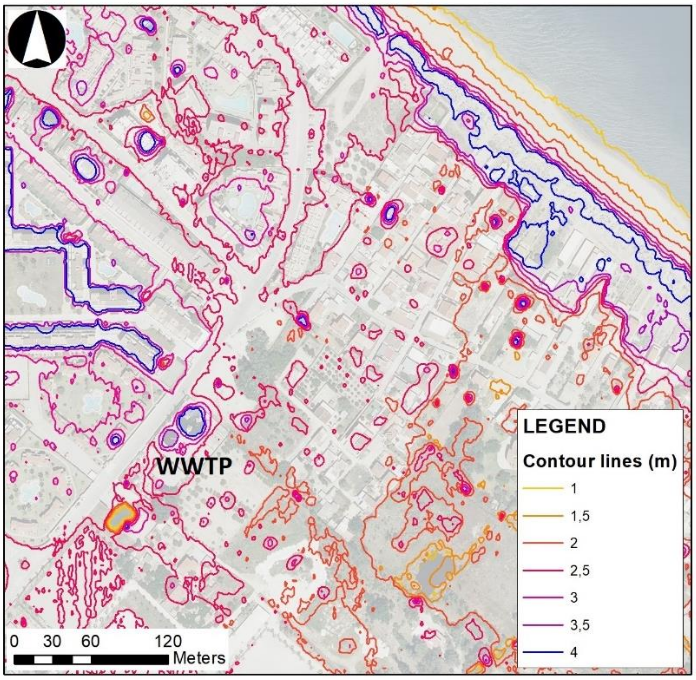

Figure 4. Map of the terrain in the study area.

3. Results and discussion

3.1. Air quality measurements

The measures taken at the wall facing the street and other important on-site reference points, except at the emission source, did not indicate measurable concentrations of either H_2S or NH_3. At the emission source the maximum concentration of H_2S recorded in a minute reached 21744 µg/m^3 and practically 100 % of the non-zero concentration values recorded at the same site were above the human perception threshold (0.47 µg/m^3). This is consistent with the panellist field olfactometry data when measured directly next to the emission source (Section 3.2).

Figure 5a gives the daily variations in emitted H_2S concentrations during the first measuring period in the 2018 high summer season. All means were clearly above the sensitive perception threshold (0.47 µg/m^3). As can be seen in this figure, residents are more likely to be affected before noon and in late evening by the peak average concentrations. This pattern can be explained by the activity of the local residents, i.e. when they use sanitary services when they start their day in the morning or come home in the evening the highest peaks can be expected. Comparing Figures 5a and 5b, it can be seen that both H_2S and influent flow rate follow a similar daily pattern and indicate that H_2S is emitted when the influent flow is pumped into the reactor.

In the anaerobic conditions (common in sewers), sulphate is reduced to hydrogen sulphide by sulphate-reducing bacteria (SRB). Since the H_2S in sewer systems is due to a microbiologically induced process and higher temperatures favour their activity, temperature could be a relevant factor correlated with the H_2S measured. Figure 5c shows the hourly mean influent wastewater temperature during the period 16 - 29 July in the 2018 high summer season. It can be seen that the temperature remains in the range 19 °C – 22°C throughout this period. Several studies have indicated this temperature range perfectly supports SRB growth and activity (Ferrentino *et al.*, 2017: Mukwevho *et al.*, 2020). A decrease in temperature from 20 to 10 °C significantly slows down SRB metabolic activity (Mukwevho *et al.*, 2020).

As can be seen in Figure 5c the daily temperature bears a certain resemblance to the flow rate daily pattern. A heatmap is included in Figure 5d with the correlation among the three parameters plus the determination coefficient (R^2) between each two variables. A positive correlation can be seen among the three variables, the strongest between H_2S and flow rate. The equation that links these two most strongly correlated variables is $H_2S(\mu g/m^3)=6.6283\ Q(m^3/d) - 160.24$

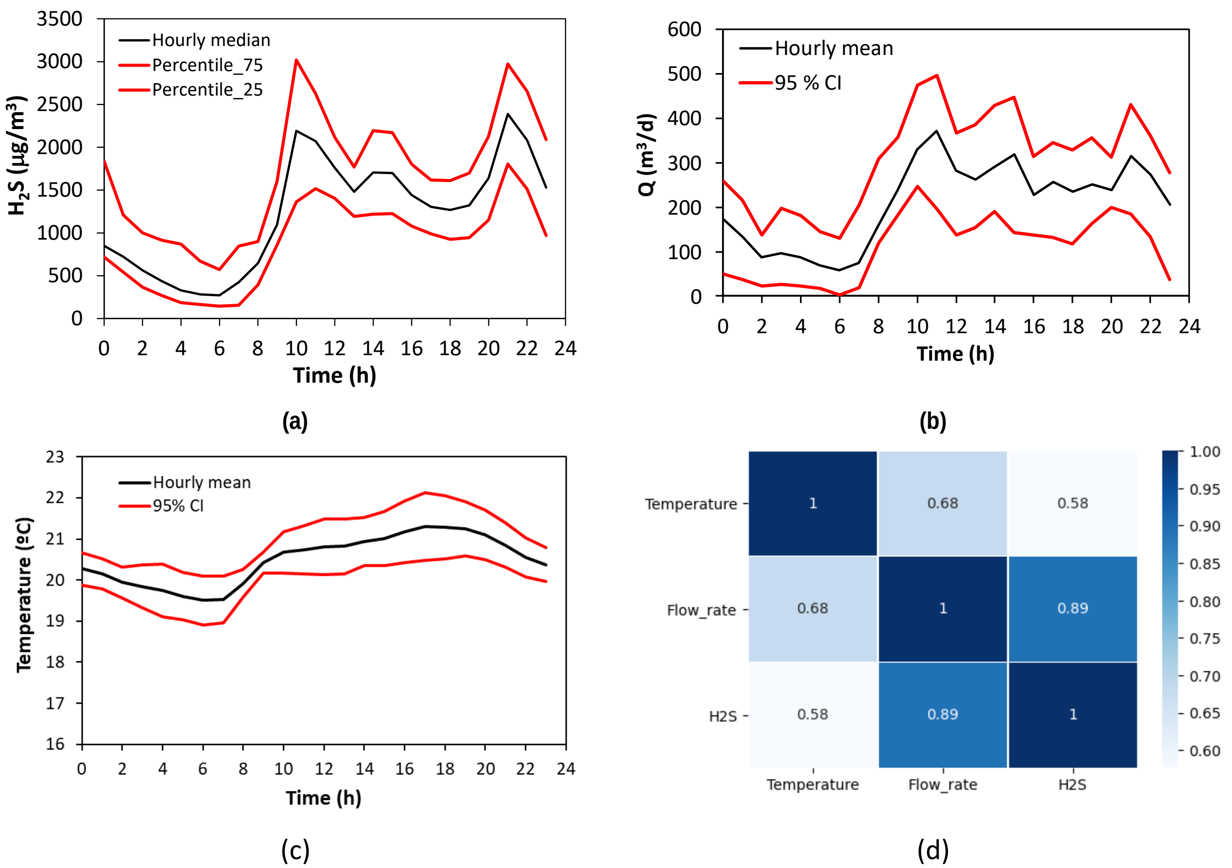

Figure 5. (a) Aggregate hourly median of hydrogen sulphide concentrations at the emission source during the measurement period (16 - 29 July). Due to the asymmetric distribution of the H_2S concentrations, the hourly median (black line) and percentiles (red lines) were plotted instead of the mean and confidence interval. **(b)** Hourly mean (black line) of the influent flow rate during the same period. The 95 % confidence interval (red lines) is also plotted for each hourly mean. **(c)** Hourly mean (black line) of the influent wastewater temperature during the same period with 95 % confidence interval (red lines) computed for each hourly mean.

(d) Heatmap showing the correlation structure (determination coefficient R^2) among H_2S, flow rate and influent wastewater temperature.

Figure 6 shows the per-minute H_2S recorded concentrations at the inlet in the high summer period 16 - 29 July in 2018 and the same period in 2019, when the inlet was submerged. Obviously, it was not possible to measure both inlets simultaneously. Despite this limitation in the comparison, it is evident from Figure 6 that with the submerged inlet H_2S concentrations were significantly lower and much more stable. Figure 6b contains a box-whisker plot of both types.

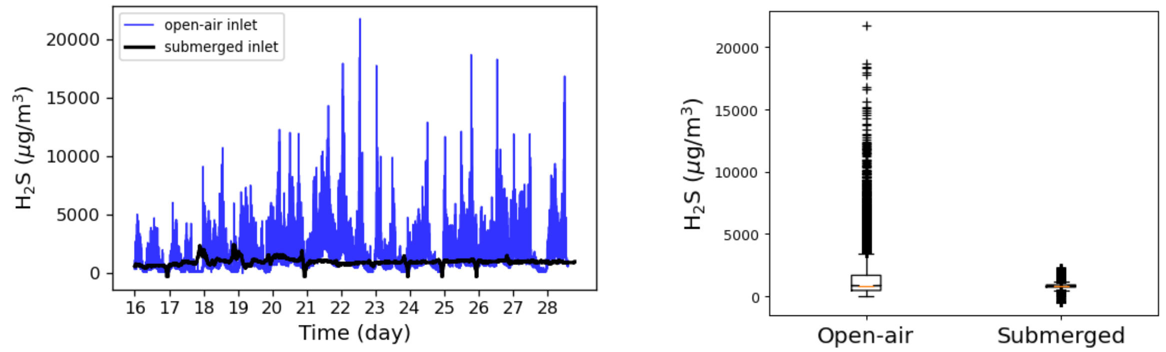

(a) **(b)**

Figure 6. (a) Time series evolution of H_2S concentration at the emission source during the measurement period 16 - 29 July in the high summer season of 2018 (open air inlet) and 2019 (submerged inlet). **(b)** Box-whisker plot corresponding to each position of the inlet. Note that the comparison corresponds to the same period in two consecutive years.

3.2. Field olfactometry

As with the gas measurements described in Section 3.1, apart from the emission source (point 2 in Figure 1b), the additional measuring points inside and outside the WWTP (shown in Figure 1b) did not show any appreciable odour concentration, if any. As can be seen in Table 1, the total average of Points 3, 4 and 5 within the premises at around 20 m from the source is less than 7 OU_E/m^3. At all points 1 and 6 to 8 m outside the premises, the average value is well below 3 OU_E/m^3 and the origin of the odour reported in point 7 was not the WWTP but a garbage truck. At the pipe entrance the maximum measured value was 71.3 OU_E/m^3 at 2018-09-05 11:30.

The mean at the emission source (point 2) was around 23.7 OU_E/m^3, based on 24 values over the measurement periods in 2018 and 2019. Wind speed and direction evidently need to be considered when interpreting the odour values, since the wind determines whether or not the airborne odorants reach a given point. Moreno-Silva *et al.* (2020) also identified wind direction as the most relevant variable in H_2S atmospheric concentrations. During the field olfactometric measurements, it was a common experience to stand a few metres from the inlet pipe while wastewater was being pumped out and yet no odour was perceived owing to the wind direction.

Table 1. Olfactometric indicators obtained from measurements at 8 points inside and outside the premises.

Olfactometric indicator	Point 1	Point 2	Point 3	Point 4	Point 5	Point 6	Point 7	Point 8
Number of olfactometric controls	5	4	5	5	2	5	5	5
Number of field-olfactometric measurement	30	24	28	28	8	28	28	28
Number of identified odours	0	3	1	2	0	0	3	0

Average percentage of measurements with odour	0	33.3	14.3	14.3	0	0	10.7	0
Average percentage of measurements ≤ 3 D/T	100	66.7	85.7	85.7	100	100	89	100
Average comprising odour (OU_E/m^3)	0	23.7	7	4.3	0	0	2.8	0
Total average (OU_E/m^3)	0	7.1	0.7	1.4	0	0	0.9	0
Maximum mean comprising odour (OU_E/m^3)	0	71.3	7	5.7	0	0	3.4	0
Minimum mean comprising odour (OU_E/m^3)	0	0	0	0	0	0	0	0

3.3. Summer wind patterns

A wind rose is superimposed on the clipped satellite map in Figure 7a showing the WWTP premises and nearby surroundings, including the residential areas to the west and north-west. The centre of the wind rose was directly over the identified odour emission source according to the field measurements. The bars on the chart represent the wind direction and speed, showing that It blows mainly towards the houses. Regarding the temporal distribution of the wind speeds and directions, Figure 7b gives the wind speed pattern filtered for the range of directions towards the dwellings (i.e., from 65 to 170 degrees). It can be understood that the wind speeds generally increase during the afternoon, reach a maximum and fall to their minimum range in the late evening, typical in coastal areas with lower wind speeds during mornings and higher velocities from noon until late evening, mainly from the sea. The observed wind pattern combined with peak wastewater flow rates in the evening match well with the AERMOD modelling results, i.e. the highest concentrations are reached in the evening and early night in the residential area and the surrounding footpath.

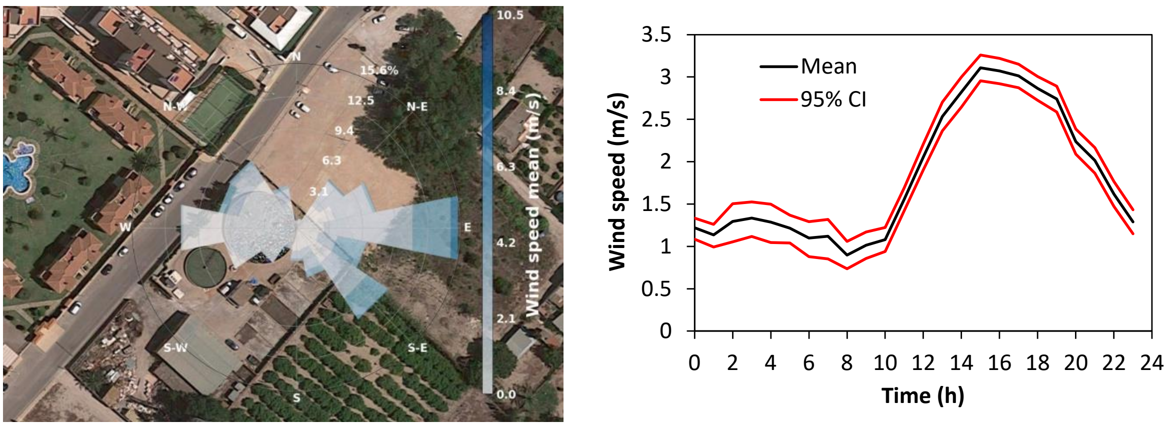

(a) (b)

Figure 7. (a) Wind rose for July 2018 representing typical high-season conditions. The wind blows chiefly west towards the dwellings. The concentric rings are labelled with the percentages of the plotted bars with respect to the total wind speed observations. **(b)** Hourly mean wind speed in July 2018. The data were previously filtered for the 65 to 170- degree range, i.e. wind from the source towards the dwellings.

3.4. Modelling results

As explained in the Materials and Methods section, the hourly maximum at the emission source was the aggregation function chosen to prevent the time averaging effect from masking the recorded one-minute peaks in H_2S concentration. The AERMOD H_2S field concentration (i.e., the one-minute H_2S field) was then corrected using the empirical peak-to-mean power-law equation to estimate the H_2S peak concentrations in the duration of a single breath (4 seconds). A more realistic prediction was thus obtained of the H_2S peaks that people in the vicinity of the WWTP could detect.

The H_2S hourly average and the peak-to-mean ratio corresponding to these integration times were calculated from the one-minute recorded H_2S concentrations at the odour source. Figure 8 shows the empirical cumulative distribution function of the peak-to-mean ratio at the source for the peak to the 1-minute measurements of the H_2S concentration and the mean to 1 hour of integration time ($t_m/t_p = 60$). The median of this empirical peak-to-mean ratio was 3.299, the 90th percentile 5.896, the 99th percentile 12.294 and maximum 16.034. According to Brancher *et al.* (2020), the maximum peak-to-mean factor near the odour source varies between 2.1 and 16.2 (using the same ratio of integration times $t_m/t_p = 60$), depending on the atmospheric stability (from very stable (Class I) to very unstable (Class V) of the Klug/Manier stability classification scheme) which influences the non-dimensional exponent (n) used in the power-law. The 90th percentile is a widely used approach to estimate sub-hourly peak concentrations in the context of odour pollution, and when it cannot be directly measured it is estimated as the long-term mean (typically hourly) by a constant factor. In Germany, this constant factor is 4 (GOAA, 2008), almost 1.5 times lower than the value obtained in this work.

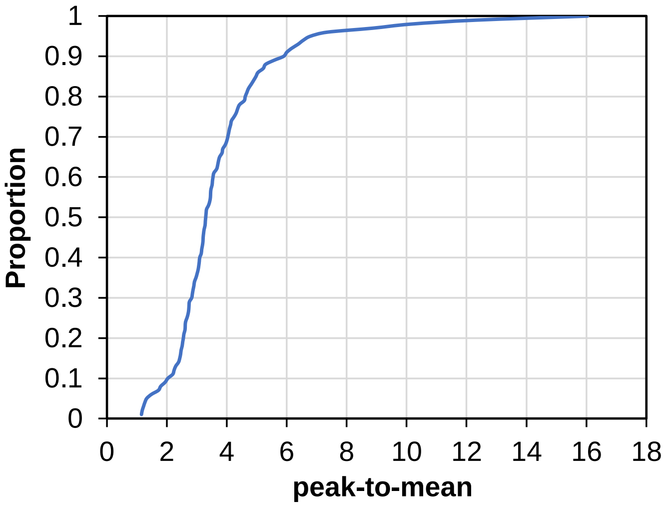

Figure 8. Empirical cumulative distribution function of the peak-to-mean ratio at the odour source (peak $\rightarrow$ t_p=1minute, mean $\rightarrow$ t_m=1 hour).

From the large day-night variation in wind speed shown in Fig. 7b, strong day-night differences in atmospheric stability can also be expected. Nights are mainly characterized by stable and very stable conditions (Dispersion Categories I and II) while during daytime hours unstable and very unstable conditions (Dispersion Categories IV and V) prevail, meaning good vertical mixing in the boundary layer.

The peak-to-mean ratio obtained by the power-law function is only valid close to the odour source and is reduced with distance from the single-point odour source due to turbulent mixing. As detailed in Schauberger *et al.* (2000), an exponential attenuation function was proposed and used to reduce the peak-to-mean ratio with distance. As demonstrated by Piringer *et al.* (2019) for unstable conditions (Klug/Manier Classes IV and V) the peak-to-mean factors starting at rather high values near the source rapidly approached 1 with distance, in agreement with the premise that vertical turbulent mixing can lead to short periods of local high ground-level concentrations while the ambient mean concentrations are low. For stable conditions (Classes II and I), the peak-to-mean ratio near the source is lowest but requires longer distances to reach 1. The neutral classes give the largest peak-to-mean factor for all distances.

Since in our case-study the closest distance from the odour source to the street is a little more than 20 meters, all possible scenarios of atmospheric stability were tested (starting from a peak-to-mean ratio of 1.62 to 6.3

at the odour source) resulting after attenuation with distance in a peak-to-mean factor lower than 1.5 outside the WWTP.

In Figure 9 the H_2S peak concentration at each of the 6400 receptor grid points in both 2-week high summer season measuring periods in 2018 are given. There was only a single incident of perception threshold of 0.47 µg/m^3. being exceeded in two specific houses in each of the depicted modelling periods. Recall that this H_2S threshold is for sensitive people, as it is one of the lowest reported values in the literature (the values published vary from 0.47 µg/m^3 to more than 100 µg/m^3). Note that the worst simulated scenario together with an unfavourable peak-to-mean ratio led to concentrations in the dwellings 10 times lower than the WHO's air quality guideline of less than 7 µg/m^3 (5 ppb) to avoid complaints. The timestamps of these punctual events were 2018-07-25 20:00 and 2018-09-06 21:00. The associated wind speeds were between 1.5 and 2 m/s and the wind directions between 80 and 90 degrees from the source towards the dwellings (Figure 5). These two modelled incidents are in line with the deductions of the temporal wind and concentration patterns shown in Figures 3 and 5.

In the second measuring campaign in 2019, none of the modelled concentrations exceeded the perception threshold at any receptor point. This result reflects the effectivity of submerging the inlet into the bioreactor to avoid splashing. The model showed that the possible downwash effects of the WWTP wall has no significant or no effect at all on the atmospheric dispersion of the pollutants emitted by the inlet due to its being only 2 m high and less than 0.5 m wide.

The H_2S results therefore indicate that it is highly unlikely that the residents perceive odours from the WWTP. In all the modelling periods only two specific dwellings to the west of the WWTP experienced peak concentrations close to the threshold concentration of odour-sensitive people (0.47 µg/m^3). This perception threshold does not mean that all those in the vicinity can clearly perceive an odour at a concentration of 0.47 µg/m^3 but indicates the lowest possible concentration some individuals can detect. The H_2S concentration that annoys most of those exposed to it is actually 10 times higher (i.e., 5 ppb or 7 µg/m^3) according to the WHO (2000), while the submersion of the influent inlet pipe makes it even more unlikely.

The results indicate that neither the onsite plant operators or nearby residents are subject to hazardous H_2S concentrations. The short-term recommended exposure limit (REL) for H_2S is defined as 13938.65 µg/m^3 (10 ppm), this being the average concentration of 15 consecutive minutes, and this does not even occur next to the emission source.

The results also revealed that capping the outlet vent and submerging the wastewater inlet stream directly into the bioreactor reduced the expected H_2S concentrations. All the modelled values during the entire period from April to June 2019 were below the perception threshold of 0.47 µg/m^3, which is why no contour map for this period is included.

When upgrading the emission source, visual protection was also installed on the top of the 2 m high wall in early 2019, consisting of a 2 m high fence of artificial green leaves. This type of protection helps mitigate any psychological effects the residents may experience when viewing an open-air WWTP. For the previous wall without the fence, the AERMOD building downwash preprocessor BPIPPRM indicated that it was useless with regard to blocking airborne dispersion from the WWTP towards the dwellings, not only because of its height but also because it is not thick enough to qualify as a 3D obstacle such as a building.

Summer is clearly the most unfavourable period, since there are more residents and more occupied dwellings, higher wastewater production and higher temperatures, which favour anaerobic processes in the sewage system (responsible for the odour compounds released). The only H_2S - values above the human perception threshold were measured at the pipe inlet, which has thus been referred to as the emission source. No humanly-detectable NH_3 values were measured even at the emission source, so that it was not considered for modelling.

(a)

(b)

Figure 9. Odour contour maps with H_2S concentrations in ppm during 2-week measuring periods in summer 2018. The threshold is shown as a white border surrounding all the contours shaded from light to dark red as the modelled concentration increases. **(a)** Contour map depicting 2-week measuring period starting from 16 July 2018. **(b)** Contour map depicting 2-week measuring period starting from 31 August 2018. Note that the plotted values are peak values (conveying information on the possible occurrence of odours) as the mean concentrations produced by AERMOD have been multiplied by the peak-to-mean ratio.

4. Conclusions

The modelling results suggest that virtually no perceptible concentrations occurred in any of the studied periods, except for two single events which were around the perception threshold of sensitive people. Considering the wind patterns, the field olfactometry measurements and the model outputs, it can be confirmed that wind direction and speed are the crucial and decisive factors that determine whether odours can be detected at a specific point. Due to its positive correlation with the activity of sulphur-reducing bacteria and the summer tourist season, which leads to the maximum annual wastewater production, temperature is thus another essential variable in odour generation.

Different points of interest in the WWTP and around the dwellings yielded no perceptible odours during the field olfactometry measurements. From the modelling results and wind patterns it can be concluded that the most unfavourable conditions for the residents are during the high summer season from approximately before noon to late evening. This is due to the wind blowing towards the dwellings, the large increase in temporary residents in the tourist area (which in turn increases the wastewater flow rate) and the high summer temperatures, which favour the activity of sulphate-reducing bacteria.

The results confirmed that the concentrations remain significantly below values hazardous to health at all the points of interest, both for the WWTP staff and the local residents. The recommended 15-minute average exposure limit for H_2S is 13938.65 µg/m^3 (10 ppm), while the maxima of the model output next to the emission source remained significantly below 1393.86 µg/m^3.

The submersion of the inlet pipe installed in 2019 proved to be effective as the associated modelling results were all below the perception threshold both inside and outside the WWTP during the 2019 modelling periods, while the direct comparison of the recorded H_2S values show a significant reduction in both concentration and variability after submersion.

The recorded H_2S concentrations showed large fluctuations around the mean value. To account for short-term odour concentrations, the empirical-based peak-to-mean approach was used. The empirical H_2S peak-to-mean ratio with integration times of 1 minute (t_p) for the peak and 1 hour (t_m), for the mean ($t_m/t_{p\,=}$ 60) ranged from 1.15 to 16.03, the median being 3.299, the 90th percentile 5.896 and the 99th percentile 12.294.

High-growing sweet-smelling plants also serve as a sight protection and are an additional odour mitigation measure. Although the perceptible pollutant concentrations reaching the footpath and the dwellings are clearly below the danger-limit values, sweet-smelling plants also filter out odours, so that the rare perception threshold exceedance events outside the premises would not be considered unpleasant.

CRediT authorship contribution statement

Andreas Luckert: Data curation, maintenance and analysis, Modelling and software, Creating data and graphic outputs, Literature research, Writing - Original draft preparation, Reviewing and Editing, Conceptualization and methodology, Field measurements, Cooperation with WWTP enterprise. **Daniel Aguado:** Supervision, Conceptualization and methodology, Literature research, Reviewing, Proof reading, Field measurements, Cooperation with WWTP enterprise. **Rafael García-Bartual:** Supervision, Conceptualization and methodology Proof reading, **Carlos Lafita:** Data supply, Field measurements, Proof reading, Contact person. **Tatiana Montoya:** Data supply, Proof reading, Contact person. **Norbert Frank:** Supervision, Proof reading.

Acknowledgments

The EPSAR (Entidad Pública de Saneamiento de Aguas de la Comunitat Valenciana) is gratefully acknowledged for its support for this work.

Funding

The authors did not receive support from any organization for this study.

Corresponding author

Correspondence to Daniel Aguado (daaggar@hma.upv.es).

Data availability

The datasets generated and/or analysed during the current study cannot be made available because of the policy of the water utility.

References

Agustine, A., Billet, S., Crumeyrolle, S., Deboudt, K., Dieudonné, E., Flament, P., Fourmentin, M., Guilbaud, S., Hanoune, B., Landkocz, Y., Méausoone, C., Roy, S., Schmitt, F.G., Sentchev, A., Sokolov, A. 2020. Impact of sea breeze dynamics in industrial and urban coastal environments. Remote sensing, 12, 648.

ATSDR (2016). Agency for Toxic Substances and Disease Registry. Hydrogen sulphide definition fact sheet. URL: https://www.atsdr.cdc.gov/toxfaqs/tfacts114.pdf.

AVAMET, AVAMET URL: https://www.avamet.org/.

AVAMET weather station Dénia Platja de Pego. AVAMET weather station "Dénia Platja de Pego". URL: https://www.avamet.org/mx-fitxa.php?id=c30m063e10.

AVAMET weather station Oliva Poble. AVAMET weather station "Oliva pople". URL: https://www.avamet.org/mx-fitxa.php?id=c25m181e02.

Baawain, M., Al-Mamun, A., Omidvarborna, H. et al. (2017) Assessment of hydrogen sulphide emission from a sewage treatment plant using AERMOD. Environ Monit Assess 189, 263 (2017). https://doi.org/10.1007/s10661-017-5983-6

Badach J., Kolasinska P., Paciorek M., Wojnowski W., Dymerski T., Gebicki J., Dymnicka M., Namiesnik J. (2018). A case study of odour nuisance evaluation in the context of integrated urban planning. Journal of Environmental Management 213, 417-424. https://doi.org/10.1016/j.jenvman.2018.02.086

Brancher M., Hieden A., Baumann-Stanzer K., Schauberger G., Piringer M. (2020). Performance evaluation of approaches to predict sub-hourly peak odour concentrations, Atmospheric Environment: X, Volume 7, https://doi.org/10.1016/j.aeaoa.2020.100076.

Carrera-Chapela, F., Donoso-Bravo, A., Souto, J.A., Ruiz-Filippi, G., 2014. Modeling the odour generation in WWTP: An integrated approach review. Water, Air, and Soil Pollution 225. doi:10.1007/s11270-014-1932-y.

Centro de Descargas del Centro Nacional de Información Geográfica (CNIG), 2018. CORINE2018 Land Cover - Spanish government access portal. URL: http://centrodedescargas.cnig.es/CentroDescargas/catalogo.do?Serie=SIOSE.

Cocci Grifoni, R., Bisegna, F., Passerini, G. 2002. A refinement of AERMOD results by means of mesoscale model simulation. 8th Conference on Harmonization within Atmospheric Dispersion Modelling for Regulatory Purposes.

CORINE Land Cover (CLC) 2018. Copernicus European Land Cover project with CORINE Land Cover (CLC) Data Base, 2018. category nomenclature. URL: https://land.copernicus.eu/user-corner/technical-library/corine-land-cover-nomenclature-guidelines/html/

Dinçer, F., Dinçer, F.K., Sarı, D., Ceylan, Ö., Ercan, Ö., 2020. Dispersion modeling and air quality measurements to evaluate the odour impact of a wastewater treatment plant in Izmir. Atmospheric Pollution Research doi:10.1016/j.apr.2020.05.018.

Dräger, Dräger Polytron 7000. URL: https://www.draeger.com/en{_}seeur/Applications/Products/Stationary-Gas-Detection-Systems/Detection-of-Toxic-Gases-and-Oxygen/Polytron-7000.

Entidad Pública de Saneamiento de Aguas Residuales (EPSAR). Technical data of WWTP Camping San Fernando, Oliva, Spain. URL: http: //www.epsar.gva.es/instalaciones/edar.aspx?id=147.

EPA and AERMIC, 2019. AERMOD model on EPA official webpage. URL: https://www.epa.gov/scram/air-quality-dispersion-modeling-preferred-and-recommended-models{#}aermod.

Fan F., Xu R., Wang D., Meng F. (2020). Application of activated sludge for odour control in wastewater treatment plants: Approaches, advances and outlooks. Water Research 181, 115915. https://doi.org/10.1016/j.watres.2020.115915

Fileni L., Matteucci G., Passerini G., Rizza U. (2018) Analysis of air pollutant emissions in a wastewater treatment plant using dispersion models J. Casares, G. Passerini, J. Barnes, J. Longhurst, G. Perillo (Eds.), WIT Transactions on Ecology and Environment, Air Pollution XXVI, vol. 230 (2018), pp. 219-230.

Halageri, N., 2012. Odour Monitoring at Wastewater Treatment Plants. University of New Orleans Theses and Dissertations, 64URL: https://scholarworks.uno.edu/td/1580.

Hvitved-Jacobsen, T., Vollertsen, J., Yongsiri, C., Nielsen, a.H., 2002. Sewer microbial processes, emissions and impacts. Sewers process and networks, 13.

GOAA, 2008. Guideline on Odour in Ambient Air GOAA. Detection and Assessment of Odour in Ambient Air. Second Version. Berlin, Germany.

Iremonger S. (2012). Environmental Publication 2012/06–A review of odour properties of H_2S Odour Threshold Investigation.

Lewkowska P., Cieślik B., Dymerski T., Konieczka P., Namieśnik J. (2016). Characteristics of odours emitted from municipal wastewater treatment plant and methods for their identification and deodourization techniques, Environmental Research,151,573-586. https://doi.org/10.1016/j.envres.2016.08.030

Li X., O'Moore L., Song Y., Bond P.L., Yuan Z., Wilkie S., Hanzic L., Jiang G. (2019). The rapid chemically induced corrosion of concrete sewers at high H2S concentration, Water Research, 162, 95-104. https://doi.org/10.1016/j.watres.2019.06

Liu J., Lu C., Huang L., Sun J., Yue P., Liu X., Kang X. (2021). Performance and economic analyses of a combined bioreactor for treating odours, volatile organic compounds, and aerosols from a landfill site, Journal of Cleaner Production, 278, 124161, https://doi.org/10.1016/j.jclepro.2020.124161.

Ma, Y., Xin, J., Zhang, X., Dai, L., Schaefer, K., Wang, S., Wang, Y., Wang, Z., Wu, F., Wu, X., Fan, G. 2021. Land-sea breeze circulation structure on the west coast of the Yellow Sea, China. Atmospheric and oceanic science letters,

14, 100003.
Moreno-Silva C., Calvo D.C., Torres N., Ayala L., Gaitán M., González L., Rincón P., Rodríguez Susa M. (2020). Hydrogen sulphide emissions and dispersion modelling from a wastewater reservoir using flux chamber measurements and AERMOD® simulations, Atmospheric Environment, 224, https://doi.org/10.1016/j.atmosenv.2020.117263
Mott A., Guo H. (2022). Odour dispersion modelling, impact criteria, and setback distances for an oil refinery plant, Atmospheric Environment, 270, https://doi.org/10.1016/j.atmosenv.2021.118879
NASA, 2019. Sentinel Satellite Cloud data before August 2019. URL: https://disc.gsfc.nasa.gov/datasets/ S5P{_}L2{_}{_}CLOUD{_}{_}1/summary?keywords=cloudbaseheight.
NASA, 2020. Sentinel Satellite Cloud data as of August 2019. URL: https://disc.gsfc.nasa.gov/datasets/ S5P{_}L2{_}{_}CLOUD{_}{_}HiR{_}1/summary?keywords=cloudbaseheight.
Nicell J.A. (2009). Assessment and regulation of odour impacts, Atmospheric Environment, 43 (1), 196-206. https://doi.org/10.1016/j.atmosenv.2008.09.033
NOAA, N., a. Integrated Global Radiosonde Archive (IGRA) - Upper air data base. URL: https://www.ncdc.noaa.gov/data-access/weather-balloon/integrated-global-radiosonde-archive.
NOAA, N., b. Integrated Surface Database (ISD) - Hourly surface weather data. URL: https://www.ncdc.noaa.gov/isd.
Oliveira, S.L.A., Corrêa, S.M. Atmospheric odour dispersion from oil refinery flare system: a case study. Environ Monit Assess 194, 563 (2022). https://doi.org/10.1007/s10661-022-10202-9
Piccardo M.T., Geretto M., Pulliero A., Izzotti A. (2022) Odour emissions: A public health concern for health risk perception, Environmental Research, Volume 204, Part B, https://doi.org/10.1016/j.envres.2021.112121
Pikaar I., Keshab I., Sharma K.R., Hu S., GernjakJürg W., Kellerand J., Yuan Z. (2014). Reducing sewer corrosion through integrated urban water management. Science, 345 (6198), 812-814. DOI: 10.1126/science.1251418
Piringer M., Knauder W.,Petz E., Schauberger G.(2015). A comparison of separation distances against odour annoyance calculated with two models, Atmospheric Environment,116,22-35,https://doi.org/10.1016/j.atmosenv.2015.06.006
Piringer M., Knauder W., Anders I., Andre K., Zollitsch W., Hörtenhuber S.J., Baumgartner J., Niebuhr K., Hennig-Pauka I., Schönhart M., Schauberger G. (2019) Climate change impact on the dispersion of airborne emissions and the resulting separation distances to avoid odour annoyance, Atmospheric Environment: X, Volume 2,100021,).
Rafiq, S., Pattiaratchi, C., Janekovic, I. 2020. Dynamics of the land-sea breeze system and the surface current response in South-West Australia. Journal of Marine Science and Engineering, 8, 931.
Schauberger G., Piringer M., Petz E. (2000). Diurnal and annual variation of the sensation distance of odour emitted by livestock buildings calculated by the Austrian odour dispersion model (AODM), Atmospheric Environment, Volume 34, Issue 28,https://doi.org/10.1016/S1352-2310(00)00240-5
Shareefdeen, Z., Singh, A., 2005. Biotechnology for Odour and Air Pollution Control. Springer, Berlin, Heidelberg, Berlin, Heidelberg. doi:https://doi.org/10.1007/b138434.
Smet, E., Lens, P., Langenhove, H.V., 1998. Treatment of Waste Gases Contaminated with Odourous Sulfur Compounds. Critical Reviews in Environmental Science and Technology 28, 89–117. URL: https://doi.org/10.1080/10643389891254179, doi:10.1080/10643389891254179.
Talbot, C., Augustin, P., Leroy, C., Willart, V., Delbarre, H., Khomenko, G. 2007. Impact of sea breeze on the boundary-layer dynamics and the atmospheric stratification in a coastal area of the North Sea. Boundary-Layer Meteorology, 125, 133-154.
Toledo M., Gutiérrez M.C., Siles J.A., Martín M.A.(2019) Odour mapping of an urban waste management plant: Chemometric approach and correlation between physico-chemical, respirometric and olfactometric variables, Journal of Cleaner Production 210, 1098-1108, https://doi.org/10.1016/j.jclepro.2018.11.109.
Walgraeve, C., Van Hufffel, K., Bruneel, J., Van Langenhove, H., 2015. Evaluation of the performance of field olfactometers by selected ion flow tube mass spectrometry. Biosystems Engineering 137, 84–94. doi:10.1016/j.biosystemseng.2015.07.007.
WHO_World Health Organization (2000). Guidelines for air quality, WHO Regional Office for Europe, Copenhagen, Denmark.
Windguru station Platja de Piles. Windguru station - Dunes Kite Piles Club / Platja de Piles, DKPiles Meteo. URL: https://www.windguru.cz/station/51.
Windguru station Playa de l'Ahuir. Windguru station - Playa de l'Ahuir, Gandia Surf. URL: https://www.windguru.cz/station/1064
Zhang T., Yan-Zhu T., Hong-Wei Y., Zhuo Chen, Xiao-Mao W., Yuefeng F. X. (2020). Study on the removal of aesthetic indicators by ozone during advanced treatment of water reuse, Journal of Water Process Engineering, 36, 101381. https://doi.org/10.1016/j.jwpe.2020.101381
Zounemat-Kermani M., Stephan D., Hinkelmann R. (2019). Multivariate NARX neural network in prediction gaseous emissions within the influent chamber of wastewater treatment plants, Atmospheric Pollution Research 10 (6), 1812-1822 https://doi.org/10.1016/j.apr.2019.07.013

Ethical approval

Not applicable.

Competing interests

The authors declare no competing interests.